References

[1]Patankar, S. V., and Sparrow, E. M., "Condensation on an Extended Surface," *Journal of Heat Transfer*, Vol. 101, 1979, pp. 434–440.

[2]Wilkins, J. E., "Condensation on an Extended Surface," *Journal of Heat Transfer*, Vol. 102, 1980, pp. 186, 187.

[3]Sarma, P. K., Chary, S. P., and Dharma Rao, V., "Condensation on a Vertical Plate Fin of Variable Thickness," *International Journal of Heat and Mass Transfer*, Vol. 31, 1988, pp. 1941–1944.

[4]Brouwers, H. J. H., "Film Condensation on Non-Isothermal Vertical Plates," *International Journal of Heat and Mass Transfer*, Vol. 32, 1989, pp. 655–663.

[5]Treviño, C., and Méndez, F., "Transient Conjugate Condensation Process on a Vertical Plate with Finite Thermal Inertia," *International Journal of Heat and Mass Transfer*, Vol. 39, 1996, pp. 2221–2230.

[6]Méndez, F., and Treviño, C., "Film Condensation Generated by a Forced Cooling Fluid," *Journal of European Mechanics, B/Fluids*, Vol. 15, 1996, pp. 217–240.

[7]Nusselt, W., "Die Oberflächenkondensation des Wasserdampfes," *Zeitschrift der Verein Deutscher Ingenieure*, Vol. 60, 1916, pp. 541–546, 569–575.

[8]Sparrow, E. M., and Gregg, J. L., "A Boundary Layer Treatment of Laminar-Film Condensation," *Transactions of the American Society of Mechanical Engineers*, Vol. 81, 1959, pp. 13–17.

[9]Koh, J. C. Y., Sparrow, E. M., and Hartnett, J. P., "The Two-Phase Boundary Layer in Laminar Film Condensation," *International Journal of Heat and Mass Transfer*, Vol. 2, 1961, pp. 69–82.

[10]Incropera, F. P., and DeWitt, D. P., *Fundamentals of Heat and Mass Transfer*, 3rd ed., Wiley, New York, 1990, p. 589.

[11]Wetzler, H., *Kennzahlen der Verfahrentechnik*, Hüthig Verlag, Heidelberg, 1985.

Heat Transfer Optimization Within Open-Ended Annular Cavities

C. P. Desai,* K. Vafai,† and M. P. Dyko‡
Ohio State University, Columbus, Ohio 43210

Nomenclature

A = exposed surface area of the annular cavity
A_h = heated area of the annular cavity
dA = elemental surface area
h = heat transfer coefficient
k = turbulent kinetic energy
L = length of the annular cavity
L_e = length of the extended computational domain
Nu = Nusselt number
n = distance normal to the surface
Pr = Prandtl number, υ/α
q = reference heat flux, applied uniform flux for the baseline case
Ra^* = modified Rayleigh number, $g\beta q R_o^4/\lambda\alpha\upsilon$
R_e = radius of the extended computational domain
R_i = radius of the inner cylinder
R_o = radius of the outer cylinder
T = temperature
T_∞ = ambient temperature
t = thickness of the annular cavity components
u_r = radial velocity
u_z = axial velocity
u_θ = azimuthal velocity
α = thermal diffusivity
β = volume expansion coefficient
ε = dissipation of turbulent K. E.
θ = angular location measured from the top
λ = thermal conductivity
υ = kinematic viscosity

Received Jan. 20, 1995; revision received Aug. 3, 1995; accepted for publication Aug. 3, 1995.

*Research Associate, Department of Mechanical Engineering.
†Professor, Department of Mechanical Engineering.
‡Graduate Student, Department of Mechanical Engineering.

Introduction

PROCESSES involving buoyancy-driven convection in open-ended cavities have been receiving a great deal of attention in recent years. This is primarily because of the fundamental nature of the geometry associated with it, which can be used to study the physical processes in a wide range of modern technological applications. These applications include, but are not limited to, fire research, cooling of the target for boron neutron capture therapy application, passive solar heating, energy conservation in buildings, cooling of electronic equipment, and modeling of thermosyphons. One of the main characteristics of buoyancy-induced flows in open-ended structures is its basic geometry, which, among other aspects, reveals the interactions and the influence of the inner (inside the cavity) and outer (the open region) flow and temperature fields. A limited amount of work has been done in the past to understand such interactions. In addition to constituting a fundamental area of research in heat transfer, understanding these interactions allows a better identification of the design parameters in a number of practical applications.

Because of the inherent nature of the geometry, natural convection in open annular cavities is a highly complex phenomenon and a theoretical analysis of this problem has to account for the three dimensionality of the flow. Hence, the amount of data reported in the literature pertaining to this geometry is very limited.[1–3]

In this work, a numerical model was developed to study natural convection cooling within an open annular cavity. The three-dimensional time-averaged equations of turbulent fluid flow and heat transfer (coupled with the k-ε model to characterize turbulence effects) were solved using a finite element method. Calculations were made for different open annular cavity configurations to investigate the influence of various geometric parameters on heat transfer characteristics of open annular cavities.

Problem Description and Solution Method

The physical model considered in the present study is an annular cavity with one end open to the ambient air. Experimental data for this configuration was obtained recently by Desai and Vafai.[4] The cavity was heated by applying a uniform heat flux to each cavity component. The equations governing the buoyancy-induced flow that develops in the surrounding air are the Reynolds' time-averaged equations of fluid motion coupled with the energy equation in the fluid and in the solid walls of the computational domain. The k-ε model was used for simulating turbulent characteristics of the convective flow.

The application of the turbulence modeling approach used in the present work to complicated forced flows involving strong and subtle flow reversal has already been demonstrated by Haroutunian and Engelman.[5] This model was found to be more accurate and computationally more effective than the k-ε model using standard wall functions. The elliptic form of the mean conservation equations (mass, momentum, and energy) were solved throughout the computational domain. The viscosity-affected region between the wall and the fully turbulent region away from the wall was modeled by means of a single layer of special elements. These specialized shape functions that were based on universal near-wall profiles accurately resolved the velocity and temperature profiles near the wall. Further details of the turbulence model can be found in an earlier paper[6] and have not been presented here for brevity.

The no-slip boundary condition for velocity was applied at all the solid walls of the computational domain. Across the vertical symmetry plane of the annular cavity, it was assumed that no exchange of energy occurs. Therefore, the boundary conditions at this symmetry plane are

$$u_\theta = 0, \quad \frac{\partial u_r}{\partial \theta} = \frac{\partial u_z}{\partial \theta} = \frac{\partial T}{\partial \theta} = \frac{\partial k}{\partial \theta} = \frac{\partial \varepsilon}{\partial \theta} = 0 \quad \text{at} \quad \theta = 0, \pi \tag{1}$$

To account for the unknown boundary conditions at the open end of the cavity, calculations were performed in a computational domain extended beyond the open end. The extension to the computational domain is basically a cylinder of radius R_e and length L_e. After extensive numerical experimentation, the following conditions were imposed at the far-field locations (based on an earlier study by Desai and Vafai[2]):

$$\frac{\partial T}{\partial r} = 0 \quad \text{at} \quad r = R_e \quad \text{and} \quad T = T_\infty \quad \text{at} \quad z = L + L_e \tag{2}$$

$$u_z = 0, \qquad \frac{\partial u_r}{\partial r} = \frac{\partial u_\theta}{\partial r} = 0 \quad \text{at} \quad r = R_e \quad \text{and} \quad u_r = u_\theta = 0$$
$$\frac{\partial u_z}{\partial z} = 0 \quad \text{at} \quad z = L + L_e \tag{3}$$

$$\frac{\partial k}{\partial r} = 0, \qquad \frac{\partial \varepsilon}{\partial r} = 0 \quad \text{at} \quad r = R_e \quad \text{and} \quad \frac{\partial k}{\partial z} = 0$$
$$\frac{\partial \varepsilon}{\partial z} = 0 \quad \text{at} \quad z = L + L_e \tag{4}$$

It was established (based on rigorous numerical experimentation) that the size of the extended computational domain required is at least three times the cavity size to eliminate the effect of the far-field boundaries on the conditions near the cavity. Finally, the interfacial boundary conditions between the cavity walls and air, the outer vertical wall and air, and also the outer cylinder and outer vertical wall were satisfied.

The set of governing equations along with boundary conditions were discretized by using a finite element formulation based on the Galerkin method of weighted residuals (FIDAP[7]). These highly coupled, nonlinear equations were solved by using an iterative solution scheme based on the segregated solution algorithm, which involves decomposition of the entire system of equations into smaller subsystems corresponding to each independent variable. Each subsystem was then solved by using an iterative solver based on a combination of the conjugate residual and conjugate gradient schemes. Convergence was assumed when the relative change in variables between consecutive iterations was less than 0.1%.

An average heat transfer coefficient, mean temperature, and average Nusselt number for the cavity were defined as

$$h_m = [q/(T_m - T_\infty)](A_h/A) \tag{5}$$

$$T_m = \int T \, dA \Big/ \int dA \tag{6}$$

$$Nu_m = h_m R_o/\lambda \tag{7}$$

Results and Discussion

To determine geometrical parameters favorable for efficient cooling of an open-ended annular cavity, the four geometries shown in Fig. 1 were studied. To evaluate the relative thermal performance of these geometries, the same total heat input was applied to each geometry. For configuration 1 (baseline case), a uniform heat flux was applied to each component of the cavity. For configuration 2, the inner cylinder heat flux was equal to the heat flux in configuration 1 while a new heat flux was applied to the endwall. For configuration 3, the uniform outer cylinder heat flux was the same as configuration 1 and a new flux over the endwall and inner cylinder was applied. The component heat fluxes for configuration 4 were also specified in a manner similar to configuration 3. The applied heat fluxes for the four geometries are shown in Fig. 1.

The dimensions of all the open annular geometries were defined by the radius ratio $R_i/R_o = 0.375$, length to outer cylinder radius ratio $L/R_o = 0.35$, and wall thickness to outer cylinder radius ratio $t/R_o = 0.025$. The thermal conductivity of the cavity components was taken to be 6000 times that of air while the thermal conductivity of the outer vertical wall was twice that of air. Results presented here correspond to a modified Rayleigh number $Ra^* = 4 \times 10^9$ and $Pr = 0.7$, which was based on the uniform heat flux applied to the components of the baseline case. These values correspond to those used in the experimental study of Desai and Vafai,[4] enabling a direct comparison for the baseline case.

For all of the computational runs, approximately 100,000 elements were required to obtain grid-independent results. Initially, the turbulence modeling approach was rigorously checked by focusing on turbulent buoyancy-driven flow in an annulus bounded by concentric, horizontal cylinders and adiabatic endwalls using both two- and three-dimensional analyses. Results were obtained for Rayleigh numbers ranging from 10^6 to 10^9, and the effects of Prandtl number and radius ratio on the flow and heat transfer characteristics were examined.[6] Good agreement was obtained between the results from this study and previously published works. Final validation of the numerical methodology used in the present work was obtained by comparison of the numerical results for the baseline case

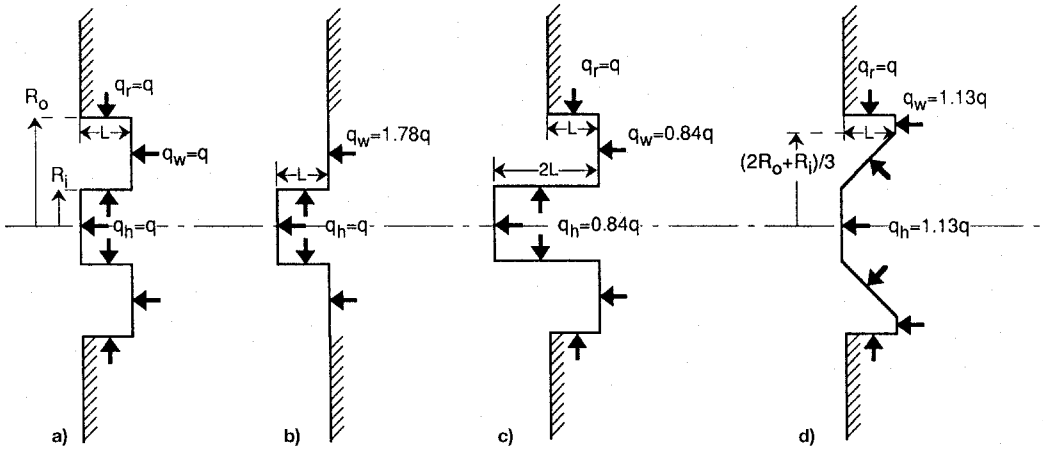

Fig. 1 Different open annular cavity configurations: a) 1, b) 2, c) 3, and d) 4.

with available experimental data.[4] For the Rayleigh number considered (4×10^9), the results agreed within 8% and displayed precisely the same trend at different axial and radial locations.

Flow Patterns

Path lines of fluid flow obtained from the numerical results for the baseline case (configuration 1) revealed that the bulk flow is characterized by fluid entering the cavity axially through lower regions of the aperture plane (the suction effect) and hot fluid exiting the cavity from the top (the ejection effect) after gaining energy from the heated internal surfaces of the cavity. The suction mechanism yields an axial inflow of ambient fluid into the lower half of the cavity. Part of this incoming fluid gets entrained into the boundary layers along the inner and outer cylinders, while the remaining fluid proceeds along the axial direction toward the endwall. Finally, the air particles that reach the endwall acquire additional energy from this surface and rise in a boundary layer along it. Fluid motion in the upper half of the symmetry plane is primarily characterized by the rising plume from the top of the inner cylinder and a strong axial outflow of hot fluid. The ejection of fluid as a buoyant jet from the top of the cavity is one of the distinct characteristics of open cavity flows. At the aperture plane, there is an outflow region just below the inner cylinder and an inflow region just above it. An upward flow along the tip of the inner cylinder was also observed. Part of this flow gets entrained into the cavity because of the local suction effect at the top of the inner cylinder while the remaining portion is entrained within the buoyant plume rising from the inner cylinder at the aperture plane.

For configuration 2, the absence of the outer cylinder basically eliminates the cavity portion of the geometry, facilitating direct interaction between the cavity components and the ambient air. Ambient air comes in direct contact with the lower portions of the endwall, rises along the endwall, and exits as a buoyant plume from the top. Unlike the baseline case, axial effects are not very significant in this configuration. For configuration 3, the flow characteristics are essentially similar to the baseline geometry, i.e., air enters the cavity through the lower regions and exits as a hot buoyant jet from the top of the cavity. The extended portion of the inner cylinder beyond the annular cavity is exposed directly to the ambient air. Hence, this portion of the inner cylinder can interact more freely with the surrounding air. However, the additional material obstructs the penetration of fluid into the cavity, especially from the lower to the upper half of the aperture plane. Finally, for configuration 4, changing the shape of the inner cylinder from cylindrical to conical has a favorable effect on the flowfield. The cylindrical shape in the other geometries results in a stagnant zone below the inner cylinder. In contrast, for configuration 4, the flow does not have to negotiate a 90-deg turn at the junction of the endwall and the cone caused by the inclined surface of the cone. The results also indicated much better penetration of ambient fluid into the cavity.

Heat Transfer Results

The average cavity temperatures and cavity Nusselt numbers for the four geometries are shown in Table 1. The cavity Nusselt number is a measure of the overall convective heat transfer rates from the cavity. The most significant advantage of configuration 2 is the elimination of the outer cylinder from the geometry. In the lower portions of the cavity, this arrangement allows cold, ambient air to come directly in contact with the endwall. This is in contrast to the other geometries where the ambient air has to penetrate the annular cavity before reaching the endwall. In the upper portions of the cavity, the presence of the restrictive upper surface of the outer cylinder for configurations 1, 3, and 4 causes the thermal boundary-layer thickness over the outer cylinder and endwall to increase as air impinges on the outer cylinder and moves axially toward the open end of the cavity. In configuration 2, on the other hand, the air rises freely as a buoyant plume above the endwall. It can be seen from Table 1 that configuration 2 has the best heat removal capabilities among the four cases considered. However, the reduced surface area (and, hence, the high applied heat flux on the endwall) also results in the highest average temperatures for this case.

Table 1 Comparison of the thermal characteristics of the different open annular geometries

Configuration	Average T, °C	Average Nu
1	96.9	52.73
2	116.1	65.21
3	87.8	53.05
4	96.0	56.76

From the flowfield results discussed earlier, it was apparent that configuration 4 allows good penetration of ambient air into the cavity. This implies improved interaction between the cavity components and the ambient air and, hence, improved thermal characteristics. Therefore, configuration 4 has higher heat transfer rates than configurations 1 and 3 (Table 1). The average temperature of the cavity components for configuration 4 is approximately equal to that for configuration 1, in spite of the reduced surface area (and, hence, higher endwall and inner cylinder heat fluxes). This is a further indication of the favorable heat transfer characteristics induced by the shape of the inner cone.

The lowest temperatures were observed for configuration 3, primarily because of the higher surface area for this geometry. The heat transfer coefficients were only slightly higher than configuration 1. The Nusselt number per unit area was the least for this geometry, indicating the poorest heat removal capabilities per unit area. Moreover, an increase in the length of the inner cylinder could result in increased weight, without providing any advantages from a heat transfer point of view.

Conclusions

Natural convective air cooling of open-ended annular cavities was investigated using a finite element analysis. Different configurations were analyzed to determine important parameters for improved thermal performance. The main conclusions of this work are summarized:

1) The annular cavity natural convection flowfield shows a strong interaction between the ambient air and the cavity air through the open end. The flow is characterized by cold, ambient air entering the cavity through the lower regions of the cavity and exiting as a hot buoyant jet from the top.

2) Configuration 2 provided the highest heat transfer rates for the cavity because of the improved interaction with the surrounding air. However, because of the reduced surface area, maximum temperatures were also encountered in this geometry.

3) Configuration 4 also showed improved flow and temperature patterns with heat transfer coefficients second only to configuration 2. Furthermore, the surface temperatures in this geometry were much lower than configuration 2.

4) Configuration 3 provides the lowest temperatures, mainly because of the higher surface area. This geometry provides the poorest option as far as cooling characteristics are concerned.

Clearly, changing the inner cylinder shape (from cylindrical to conical) improves the flow patterns and, hence, the cooling characteristics. On the other hand, elimination of the outer cylinder has the highest heat removal capabilities if the limiting temperature tolerances can be raised.

References

[1]Vafai, K., and Ettefagh, J., "Axial Transport Effects on Natural Convection Inside of an Open Ended Annulus," *Journal of Heat Transfer*, Vol. 113, No. 3, 1991, pp. 627–634.